Optics Letters

Heterogeneous integration of lithium niobate and silicon nitride waveguides for wafer-scale photonic integrated circuits on silicon

Lin Chang,[1,*] Martin H. P. Pfeiffer,[2] Nicolas Volet,[1] Michael Zervas,[2,3] Jon D. Peters,[1] Costanza L. Manganelli,[1,4] Eric J. Stanton,[1] Yifei Li,[1,5] Tobias J. Kippenberg,[2] and John E. Bowers[1]

[1]Department of Electrical and Computer Engineering, University of California, Santa Barbara, California 93106, USA
[2]École Polytechnique Fédérale de Lausanne (EPFL), 1015 Lausanne, Switzerland
[3]Ligentec, 1015 Lausanne, Switzerland
[4]Scuola Superiore Sant'Anna, Istituto Tecip, Via G. Moruzzi 1, Pisa 56124, Italy
[5]Department of Electrical and Computer Engineering, University of Massachusetts Dartmouth, Dartmouth, Massachusetts 02032, USA
*Corresponding author: linchang@ece.ucsb.edu

Received 13 December 2016; revised 20 January 2017; accepted 21 January 2017; posted 24 January 2017 (Doc. ID 282456); published 13 February 2017

An ideal photonic integrated circuit for nonlinear photonic applications requires high optical nonlinearities and low loss. This work demonstrates a heterogeneous platform by bonding lithium niobate (LN) thin films onto a silicon nitride (Si_3N_4) waveguide layer on silicon. It not only provides large second- and third-order nonlinear coefficients, but also shows low propagation loss in both the Si_3N_4 and the LN-Si_3N_4 waveguides. The tapers enable low-loss-mode transitions between these two waveguides. This platform is essential for various on-chip applications, e.g., modulators, frequency conversions, and quantum communications. © 2017 Optical Society of America

OCIS codes: (190.4390) Nonlinear optics, integrated optics; (130.3730) Lithium niobate; (040.6040) Silicon.

https://doi.org/10.1364/OL.42.000803

For decades, lithium niobate (LN) has become the most commonly used nonlinear material in photonics [1], since it has a large electro-optic effect ($r_{33} > 30$ pm/V), a high second-order nonlinear coefficient (27 pm/V), and a broad transparency window (0.35–4.5 μm) [2]. It is widely used for electro-optic modulators [3,4], three-wave-mixing wavelength converters [5,6], and optomechanical cavities [7]. Recently, there has been great interest in integrating LN devices in photonic integrated circuits (PICs) [8–10]. Compared to bulk LN devices, integrated ones have much smaller scale. This not only shrinks the footprint of the optical system but also enhances the nonlinear effects due to the higher photon density [10], potentially reducing the power budget for modulation and wavelength conversion.

Among integrated-photonics areas, silicon (Si) photonics has the highest potential for mass-market applications in industry [11]. However, one limitation for it is that, even though Si, Si_3N_4, and SiO_2 have been widely applied based on their third-order optical nonlinearities (Kerr effect, $\chi^{(3)}$), usually they do not have any second-order nonlinearities ($\chi^{(2)}$) or electro-optic effect, due to their centrosymmetric crystal structures or amorphous nature. As a result, it is challenging to achieve many important functions, e.g., electro-optic modulation and three-wave mixing on the Si platform. To introduce a significant second-order nonlinearity, there have been many attempts to integrate nonlinear materials onto Si, especially LN [8,12]. One commonly used technique is to bond thin film LN fabricated by an ion slice method [13] onto a Si-on-insulator (SOI) wafer, where Si ridges are used for guiding the mode in the LN-Si waveguide. However, this approach suffers from several shortcomings. First, the losses of these heterogeneous waveguides are higher (>2.5 dB/cm) [12,14] than conventional bulk LN waveguides (<1 dB/cm) [15]. Second, Si is absorptive at wavelengths shorter than 1.1 μm, a characteristic that is, however, of great importance for many applications [16,17]. Finally, the refractive index of Si (~3.48) is much higher than that of LN (~2.14 for extraordinary polarization at C band). This dramatically decreases the confinement factor in the LN core, and this decrease is detrimental for nonlinear interactions. Even though this can be reduced if narrow and thin Si ridges are used [12], it adds difficulties in fabrication. Other materials such as Ta_2O_5 have also been used to form the heterogeneous waveguide with LN [9]. However, reported loss values for these waveguides are still relatively high. More importantly, tapers for mode conversion between different material cores have not been demonstrated due to their index-matching problem.

Compared to Si, Si_3N_4 has lower material loss and a broader transparency window (0.4–6.7 μm) [18], and, most importantly, does not suffer from two-photon absorption. Si_3N_4 waveguides are popular for nonlinear photonics, such as Kerr frequency comb and soliton generation [19]. Recently, a novel photonic Damascene process has been developed for fabricating high-confinement Si_3N_4 waveguides with high

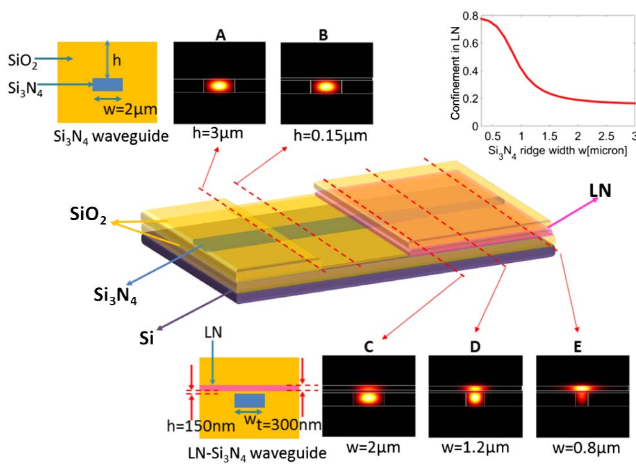

Fig. 1. Schematic structure of a tapered mode converter connecting the two types of waveguides. The top and bottom areas show schematics of the waveguide cross-sections and simulated profiles of the fundamental TE modes at 1540 nm. Inset is the simulated confinement factor in the LN layer for LN-Si_3N_4 hybrid waveguides calculated as a function of the Si_3N_4 rib width.

yield, mitigating common fabrication challenges [20]. The efficient stress control of this method can provide thick Si_3N_4 waveguides free of cracks, an essential prerequisite to achieve index matching with a bonded LN layer in a heterogeneous waveguide. Moreover, the planar top surface of this process facilitates integration of LN film by wafer bonding. Owing to the fully cladded nature, the Si_3N_4 waveguide fabricated using the Damascene process shows low propagation loss (0.11 dB/cm), a benefit for $\chi^{(3)}$ interactions, according to our previous results [21]. In this work, Si_3N_4 is used as the rib of the heterogeneous waveguide formed with LN film. Because the refractive index of Si_3N_4 (1.98) is slightly smaller than that of LN, the mode of the hybrid waveguide can be highly confined in the LN core (see Fig. 1). Owing to the low-loss nature of the Si_3N_4 ridge and the low field intensity at the boundaries and sidewalls, such a LN-Si_3N_4 waveguide can achieve low propagation loss [9,12]. An alternative approach for LN-SiN low-loss waveguides is to deposit SiN on a LN film as shown in our previous work [10]. However, the Damascene process provides a high-quality stoichiometric Si_3N_4 layer, which can also be thicker for improved index matching for low-loss mode transitions between the Si_3N_4 and LN-Si_3N_4 waveguides. This platform provides strong $\chi^{(2)}$ and $\chi^{(3)}$ coefficients ($\gamma \sim 1.4\ W^{-1}\ km^{-1}$ for this work), high confinement factors, low propagation, and coupling losses for waveguides.

The heterogeneous platform presented here consists of two types of waveguides, both illustrated in Fig. 1. The fully cladded Si_3N_4 waveguide for $\chi^{(3)}$ nonlinear interaction is 850 nm high and ~2 μm wide to achieve anomalous group velocity dispersion at C band. Another type is the LN-Si_3N_4 waveguide for $\chi^{(2)}$ applications, consisting of a 300-nm-thick LN layer separated from a Si_3N_4 core by a 150-nm-thin SiO_2 spacer. Such geometry matches the indices of these two layers.

The schematic cross-section of the LN-Si_3N_4 waveguide is shown in Fig. 1. Because the Si_3N_4 waveguide and the LN layer have nearly the same index, confinement factors in these two cores are sensitive to Si_3N_4 ridge width, shown in the top right inset of Fig. 1. The ridge width is designed to be 0.8 μm, corresponding to a confinement factor of ~0.6 in LN core.

A mode converter is designed to enable low-loss mode transition between the two types of waveguides, and a schematic is shown in the center of Fig. 1. The Si_3N_4 input waveguide is 2 μm wide with 3-μm SiO_2 top cladding (A), and input light then passes through an abrupt change of the upper cladding to 150 nm (B). After entering the bonded area with a LN film top, the width of the Si_3N_4 ridge decreases linearly from 2.0 μm (C) to 0.8 μm (E), adiabatically transitioning the majority of the mode upward into the LN layer. The evolution of simulated mode distributions (performed with FIMMWAVE [22]) for different waveguide geometries is shown in Fig. 1, at 1540 nm wavelength. According to simulations, the loss per LN facet (from A to E) is 0.9 dB, due to the abrupt index change between the Si_3N_4 and heterogeneous waveguides (B to C). Here a 150-nm-thick SiO_2 spacer is introduced to reduce this index change. Further increasing the spacer thickness to 300 nm is expected to reduce the loss to 0.4 dB per facet, but this will also increase the optical mode size. This tradeoff can be adjusted depending on the application.

The device fabrication process is schematized in Fig. 2. The photonic Damascene process [20] is used to fabricate the Si_3N_4 waveguide devices on a 100-mm substrate and provide local openings with planar surface for LN bonding. At first, an 850-nm-thick layer of nearly stoichiometric Si_3N_4 is deposited by low-pressure chemical vapor deposition on a prestructured substrate. The substrate includes not only the waveguide pattern but also a dense stress-release pattern, to avoid the formation of cracks during the Si_3N_4 deposition that cause high scattering loss. Chemical-mechanical polishing is used to remove excess Si_3N_4 after deposition, creating a planar top surface across the wafer. A 3-μm-thick SiO_2 layer is then deposited on Si_3N_4 as the top cladding. A scanning electron micrograph (SEM) of the cross-section of this Si_3N_4 waveguide is shown in Fig. 3(a). To reduce the surface roughness in preparation for

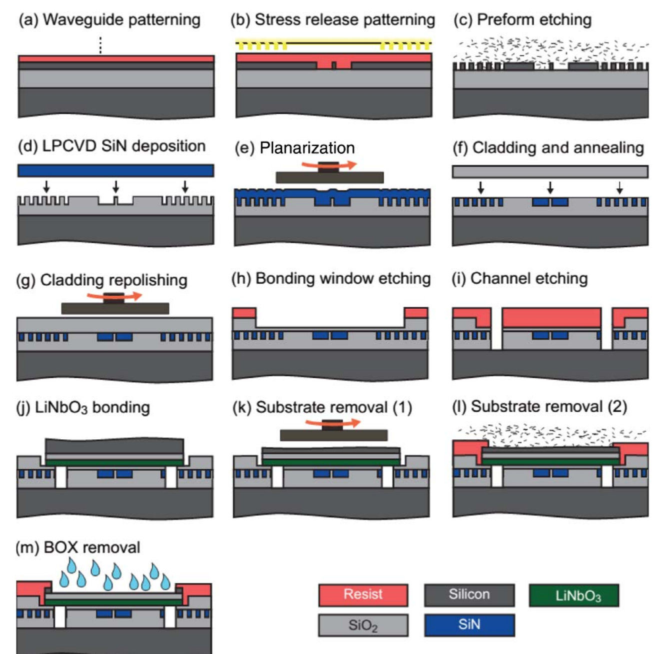

Fig. 2. Fabrication procedure for the LN-Si_3N_4 platform.

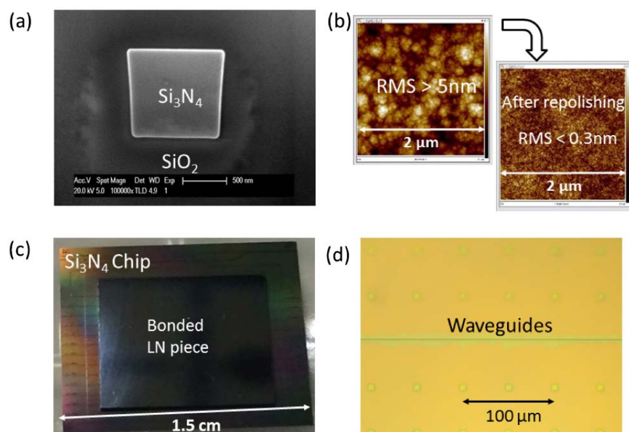

Fig. 3. (a) SEM cross-section of the Si_3N_4 waveguide. (b) Roughness testing results after SiO_2 deposition and repolishing. (c) Top view of integrated LN-Si_3N_4 chip. (d) Bonded area after substrate and BOX layer removal.

bonding, the deposited SiO_2 cladding layer is repolished. Figure 3(b) shows the roughness measurement of the as-deposited low temperature SiO_2 film as well as after the repolishing step. The bonding area is then opened by dry etch, leaving a thin SiO_2 layer as spacer. Additionally, vertical channels are patterned in these areas to release the gas during bonding. After that, a chip (purchased from NANOLN) consisting of a 300-nm-thick *x*-cut LN film on a 2-μm-thick buried SiO_2 on a Si substrate is bonded onto the opened area after surface plasma activation. The bonded sample is then annealed to enhance the bonding strength. The integrated chip is shown in Fig. 3(c). Finally, mechanical polishing, dry etch, and buffered hydrofluoric acid have been used to remove the Si substrate and buried oxide (BOX) layer, leaving only the LN film on chip in the open area, as shown in Fig. 3(d).

For characterizing the devices, a tunable single-frequency CW laser (Keysight 81642A) with spectral range of 1.51–1.64 μm and linewidth ~0.1 MHz is used as the light source. Collimated light passes through a polarizer (Thorlabs PCB-2.5-1550) aligned to efficiently excite the TE-polarized mode of the waveguide. A focusing lens (Thorlabs C230TM-C) is used for the input coupling, and a lensed fiber couples the light out of the device. An optical power sensor (Keysight 81634B) is used to monitor the transmitted power.

The testing structure used here is a 1-cm-long heterogeneous waveguide, with two tapers connecting to the Si_3N_4 waveguides. TE polarized light is coupled in and out through the Si_3N_4 waveguides. Compared to the reference Si_3N_4 waveguide with the same length, the insertion loss (fiber to fiber) of the heterogeneous waveguide is ~2 dB larger around C band, shown in Fig. 4. There are small ripples for the heterogeneous waveguide spectrum, possibly due to the taper reflections.

Here, the insertion loss for the reference and the test structures are denoted α_{ref} and α_{test}, respectively, and their propagation loss is denoted by α_{SiN} and α_{heter}, respectively. The following equations define the total insertion loss:

$$\alpha_{\mathrm{ref}} = \alpha_{\mathrm{SiN}} + \alpha_c, \tag{1}$$

$$\alpha_{\mathrm{test}} = \alpha_{\mathrm{heter}} + 2\alpha_{\mathrm{AB}} + 2\alpha_{\mathrm{BC}} + \alpha_c, \tag{2}$$

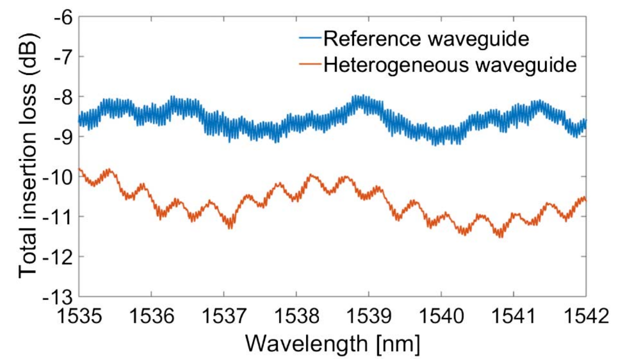

Fig. 4. Spectra of total insertion loss for the reference waveguide (blue) and heterogeneous waveguide (red).

where α_{AB} and α_{BC} are the losses at the A–B and B–C boundaries in Fig. 1, and α_c is the coupling loss in and out of the chip.

The propagation loss for the heterogeneous waveguide is obtained by subtracting Eq. (2) from Eq. (1), as follows:

$$\alpha_{\mathrm{heter}} = \alpha_{\mathrm{SiN}} - 2\alpha_{\mathrm{AB}} - 2\alpha_{\mathrm{BC}} - (\alpha_{\mathrm{ref}} - \alpha_{\mathrm{test}}). \tag{3}$$

The value of $\alpha_{\mathrm{ref}} - \alpha_{\mathrm{test}}$ is obtained from the testing results of Fig. 4 and α_{SiN} by the prementioned measurements of resonators (0.11 dB/cm * 1 cm), assuming that $\alpha_{\mathrm{AB}} + \alpha_{\mathrm{BC}} \cong 0.9$ dB as supported by simulations. The calculated propagation loss for the heterogeneous waveguide is (0.2 ± 0.4) dB/cm. Considering that the coupling loss varies among waveguides, this method may have an extra uncertainty. Here the Fabry–Perot-based method is also used, and a loss of (0.3 ± 0.6) dB/cm is extracted, resulting in good agreement. Such a low propagation loss is comparable to the loss of a bulk LN waveguide [15]. Considering that the waveguide area is more than 1 order of magnitude smaller than that of bulk waveguides, these waveguides can improve the efficiency for nonlinear applications by the same proportion without sacrificing additional propagation loss.

In conclusion, a heterogeneous platform on Si is demonstrated with large $\chi^{(2)}$ and $\chi^{(3)}$ coefficients by bonding a LN film onto thick Si_3N_4. With careful design of the waveguide geometry and by using advanced fabrication techniques, high confinements and low propagation losses have been achieved both for Si_3N_4 and LN-Si_3N_4 waveguides, with low-mode-transition loss from using a taper. Therefore, this platform is promising for the wide range of chip-level nonlinear applications on Si.

Funding. Defense Sciences Office (DARPA) MTO DODOS (HR0011-15-C-055); Seventh Framework Programme (FP7) (iQUOEMS 323924); Swiss National Science Foundation.

REFERENCES

1. R. W. Boyd, *Nonlinear Optics*, 3rd ed. (Academic, 2008).
2. J. E. Toney, *Lithium Niobate Photonics* (Artech House, 2015).
3. A. J. Mercante, P. Yao, S. Shi, G. Schneider, J. Murakowski, and D. W. Prather, Opt. Express **24**, 15590 (2016).
4. S. Jin, L. Xu, H. Zhang, and Y. Li, IEEE Photon. Technol. Lett. **28**, 736 (2016).

5. R. Geiss, S. Saravi, A. Sergeyev, S. Diziain, F. Setzpfandt, F. Schrempel, R. Grange, E. B. Kley, A. Tünnermann, and T. Pertsch, Opt. Lett. **40**, 2715 (2015).
6. S. Kurimura, Y. Kato, M. Maruyama, Y. Usui, and H. Nakajima, Appl. Phys. Lett. **89**, 191123 (2006).
7. R. Wang and S. A. Bhave, Opt. Express **23**, 23072 (2015).
8. L. Chen, Q. Xu, M. G. Wood, and R. M. Reano, Optica **1**, 112 (2014).
9. P. Rabiei, J. Ma, S. Khan, J. Chiles, and S. Fathpour, Opt. Express **21**, 25573 (2013).
10. L. Chang, Y. Li, N. Volet, L. Wang, J. Peters, and J. E. Bowers, Optica **3**, 531 (2016).
11. M. J. R. Heck, J. F. Bauters, M. L. Davenport, J. K. Doylend, S. Jain, G. Kurczveil, S. Srinivasan, Y. Tang, and J. E. Bowers, IEEE J. Sel. Top. Quantum Electron. **19**, 6100117 (2013).
12. P. O. Weigel, M. Savanier, C. T. DeRose, A. T. Pomerene, A. L. Starbuck, A. L. Lentine, V. Stenger, and S. Mookherjea, Sci. Rep. **6**, 22301 (2016).
13. P. Rabiei and P. Gunter, Appl. Phys. Lett. **85**, 4603 (2004).
14. J. Chiles and S. Fathpour, Optica **1**, 350 (2014).
15. K. R. Parameswaran, R. K. Route, J. R. Kurz, R. V. Roussev, M. M. Fejer, and M. Fujimura, Opt. Lett. **27**, 179 (2002).
16. S. Bloom, E. Korevaar, J. Schuster, and H. Willebrand, J. Opt. Netw. **2**, 178 (2003).
17. E. J. Stanton, A. Spott, M. L. Davenport, N. Volet, and J. E. Bowers, Opt. Lett. **41**, 1785 (2016).
18. P. T. Lin, V. Singh, H. G. Lin, T. Tiwald, L. C. Kimerling, and A. M. Agarwal, Adv. Opt. Mater. **1**, 732 (2013).
19. D. J. Moss, R. Morandotti, A. L. Gaeta, and M. Lipson, Nat. Photonics **7**, 597 (2013).
20. M. H. P. Pfeiffer, A. Kordts, V. Brash, M. Zervas, M. Geiselmann, J. D. Jost, and T. J. Kippenberg, Optica **3**, 20 (2016).
21. L. Wang, L. Chang, N. Volet, M. H. P. Pfeiffer, M. Zervas, H. Guo, T. J. Kippenberg, and J. E. Bowers, Laser Photon. Rev. **10**, 631 (2016).
22. Photon Design, https://www.photond.com.

128.111.239.206 {ts '2017-06-28 14:09:05'}